New Journal of Physics
The open–access journal for physics

Synergistic erosion process of hydrocarbon films: a molecular dynamics study

P N Maya[1], U von Toussaint[2,3] and C Hopf[2]

[1] Institute for Plasma Research, BHAT, Gandhinagar, Gujarat, 382428 India

[2] Max-Planck-Institut für Plasmaphysik, Boltzmann Straße 2, 85748 Garching, Germany

E-mail: udo.v.toussaint@ipp.mpg.de

New Journal of Physics **10** (2008) 023002 (15pp)
Received 8 November 2007
Published 6 February 2008
Online at http://www.njp.org/
doi:10.1088/1367-2630/10/2/023002

Abstract. Fundamental processes leading to the erosion of hydrocarbon films due to energetic argon ions and hydrogen atoms have been investigated using molecular dynamics simulations. A generic mechanism has been identified for carbon erosion due to energetic (150 eV) argon ions in the presence of sub-eV hydrogen atoms. This surface erosion process, which we call *hydrogen enhanced physical sputtering* (*HEPS*), is primarily a physical sputtering mechanism, enhanced due to the screening effect of hydrogen atoms. The energetic argon ions create open bonds within their penetration range. The hydrogen atoms passivate the open bonds created within the first few atomic layers. Subsequent ion bombardment causes the breaking of C–C bonds within and beyond the H penetration range. The steric effect of H atoms bound to the top layer of carbon atoms prevents the re-attachment of the broken bonds, and this leads to unsaturated molecule emission from the surface. The kinetic energy of the emitted molecules is above thermal energy and the emission takes place within 5 ps after the ion impact.

[3] Author to whom any correspondence should be addressed.

Contents

1. Introduction and motivation

Hydrogen isotope retention in carbon-based plasma-facing materials is a potentially limiting constraint in the long-term operation of fusion reactors [1]–[3]. As of now there is no real substitute for carbon for handling high heat fluxes in the divertors of tokamaks. The interaction of hydrogen with carbon-based plasma-facing components (PFCs) leads to their erosion by both momentum transfer processes (physical sputtering) and chemical reactions [4]. The various eroded hydrocarbon (C_xH_y) radicals get deposited in the form of a thin layer on the inner surface of fusion devices [5]–[9]. Future reactors will use tritium as fuel, and hence the tritium inventory build-up may lead to various safety issues limiting the operation as well as to economic constraints due to fuel retention.

The PFCs interact with both energetic and thermal hydrogen species. In order to understand and quantify the influence of the energetic particles on carbon erosion, various experiments employing hydrogen ion beams have been performed [10, 11]. The experiments showed that the resulting erosion rates at moderate energies are far higher than expected from physical sputtering. The same enhancement was also found in experiments on the erosion of graphite or amorphous hydrocarbon films (a-C:H) where the kinetic energy and the chemical reactivity were supplied by two independent particle fluxes, a beam of energetic argon ions and another flux of thermal hydrogen atoms [12]–[16]. The resulting erosion rates were higher than both the expected *physical sputtering* rate as well as the *chemical erosion* rate due to the hydrogen atoms, which in some experimental cases was zero due to the sample being at ambient temperature. In order to indicate that both momentum transfer processes and chemical reactions play a role in this enhanced erosion process, it is commonly referred to as *chemical sputtering* [4].

Chemical erosion of carbon by hydrogen is a thermally driven process which does not require any energetic species and has been studied using thermal hydrogen atom beams [17]. An incident hydrogen atom creates a radical site by abstracting a bound hydrogen from the surface. The radical site relaxes via the emission of a neighbouring CH_3 radical. The molecule ejection is a thermally activated process with an energy barrier of 1.6 eV. Therefore, it happens only at elevated surface temperatures.

Physical sputtering of a-C : H films by hydrogen ions has been extensively investigated in the past both by experimental [18] and computational means [19]–[21]. It is essentially an elastic collision process, in which the momentum of the energetic incident atom is either transferred directly to the sputtered atom or by indirect means, i.e. by creating primary knock-on atoms

followed by a collision cascade. The sputtered particles originate from the first few atomic layers, and the sputtering process occurs within a few picoseconds' time. There exists an energy threshold for this process and the energy distribution of the sputtered species is well above thermal energies.

Another recently described erosion mechanism, termed *swift chemical sputtering*, has been identified by Salonen *et al* [22] using molecular dynamics simulations . In this process, incident ions with energies down to about 2 eV cause the kinetic emission of hydrocarbon radicals from a-C:H films. The process has been reported for both hydrogen and helium ions [23, 24] and is therefore considered by some as a special case of physical sputtering [25]. It is, however, also not able to explain the high experimental yields of [13, 14].

No single definition for the term *chemical sputtering* can be found in the literature yet. For an overview of the chemical sputtering of carbon see [4]. In that paper, chemical sputtering is defined in a very general sense as any process in which ion bombardment promotes chemical reactions which lead to an enhancement of the erosion rate over both the physical sputtering rate and the rate caused by the same flux of the reactive particles at thermal energies. The chemical sputtering of graphite by D^+, D_2^+ and D_3^+ ions in the very low energy range between 5 and 60 eV per D was recently investigated both experimentally and with molecular dynamics simulations and good agreement was found [26]–[28].

Chemical sputtering by two individual beams of energetic noble gas ions and thermal hydrogen atoms was studied in particle beam experiments [13]–[16] for different Ar energies and a varying hydrogen to argon flux ratio of between 0 and ≈ 500. It was observed that the additional flux of hydrogen atoms leads to a dramatic increase in the sputtering yield. Variation of the Ar^+ energy in the range from 20 to 800 eV at a constant H/Ar^+ flux ratio of 400 showed an energy dependence which could not be explained by a pure physical sputtering mechanism. Hopf *et al* [13] proposed a model which explains the observed chemical sputtering by C–C bond breaking due to energetic Ar ions and the passivation of the broken bonds by thermal H atoms followed by the diffusion of the saturated volatile molecules to the surface. However, the adequacy of this phenomenologically derived atomistic picture of the erosion mechanism is not clear. Therefore, in the present study, we perform molecular dynamics simulations to gain insight into the atomistic picture of this synergistic erosion process which is not accessible by experiments. In the simulations amorphous hydrocarbon (a-C:H) films are bombarded by 150 eV Ar ions in a background of low energy (0.5 eV) hydrogen atoms.

Section 2 describes the details of the simulation for the sample preparation and the bombardment studies, followed by the results in section 3. The results are discussed in section 4. In section 5, the conclusions are presented together with an outlook.

2. Simulation method

2.1. Sample preparation and characterization

A molecular dynamics simulation code, Hydrocarbon Parallel Cascade (HCParCas version V3.22), has been used which employs a fifth-order predictor–corrector Gear algorithm to calculate the positions and velocities of particles using adaptive time steps [29]. The a-C:H samples were prepared by annealing a collection of carbon and hydrogen atoms using the Brenner potential for C–H and C–C interactions [30, 31]. The sample preparation was similar to the preparation method given in [32].

The initial sample contained 1000 randomly positioned atoms with the random placement restricted to interatomic distances above a threshold distance of 1.1 Å. This approach avoids the problem of persistent long range correlations in crystalline samples amorphized by particle bombardment. The sample was annealed several times in temperature cycles from 300 to 4000 K and back to 300 K at a temperature rate of 0.01 K fs^{-1}. Berendsen scalings [33] were used for the temperature and pressure control, and periodic boundary conditions were applied along the xyz-directions of the sample. After 50 ns annealing at 300 K the periodic boundary along the z-axis was removed, followed by another 7 ns of equilibration time to cure artificially broken bonds. Atoms within a distance of 3 Å of the bottom of the cell were fixed for mimicking the effect of an underlying bulk layer. Also, the prolonged relaxation helped to identify and remove H_2 molecules formed within the sample during annealing. As the next step of the surface preparation, the sample was bombarded with low energy (5 eV) Ar atoms with random impact angles and locations to get rid of loosely bound C atoms on the surface, which arise due to the removal of periodic boundary conditions along the z-axis.

Finally, to mimick the experimental conditions, the surface was exposed to a flux of thermal H atoms. After another 12 ns of annealing, the sample with dimensions of $14 \times 14 \times 28$ Å^3 had 930 atoms with an H/C ratio of 0.61 and a density of 1.750 g cm^{-3}. Very similar values—H/C = 0.64 and a density of 1.7 g cm^{-3}—have been reported for a-C:H layers deposited from ethylene plasma discharges [34]. The fractions of 3-fold and 4-fold coordinated carbon atoms were 60 and 37%, which is in good agreement with the experimental data for a-C:H films with properties intermediate between hard and soft [35]. The amorphous nature of the sample has been characterized by the radial density distribution function (RDF) of the carbon atoms computed for the carbon network by

$$g(r) = \frac{V}{4\pi r^2 N^2} \left\langle \sum_i \sum_{i \neq j} \delta(\vec{r} - \vec{r}_{ij}) \right\rangle, \tag{1}$$

where V is the volume, N is the number of particles in the system, and $\vec{r}_{ij}$ is the distance between particles i and j. The RDF gives the conditional probability of finding an interparticle distance of r. Thus $g(r)$ provides a measure of local spatial ordering.

2.2. Bombardment simulations

The sample was bombarded with monoenergetic 150 eV Ar atoms at an angle of 45° with respect to the surface normal and at random azimuthal angles. The more generic off-normal impact angle was chosen to avoid any particularities which may be associated with the special case of normal incidence, and at the same time resembles the conditions in fusion experiments more closely. The Ar interactions with carbon and hydrogen atoms were modelled using additive pair-potentials of the Ziegler–Biersack–Littmark type [36].

The bombarding atoms were initialized at a height of 7 Å above the surface, which is beyond the largest cut-off radius of 4.5 Å of all the potentials used in this simulation. The Ar bombardment simulations were run for 5 ps. In the sample, the energetic argon atoms were typically thermalized within 0.5 ps after the impact, and thereafter the sample was relaxed for another 4.5 ps. Monoenergetic hydrogen atoms of 0.5 eV energy were incident upon the Ar bombarded surface with 45° polar and random azimuthal angles. The simulation time for a single H bombardment was 5 ps, and 50 H atoms were incident for each Ar atom. We refer to one such sequence of one Ar impact followed by 50 hydrogen atoms as one co-bombardment

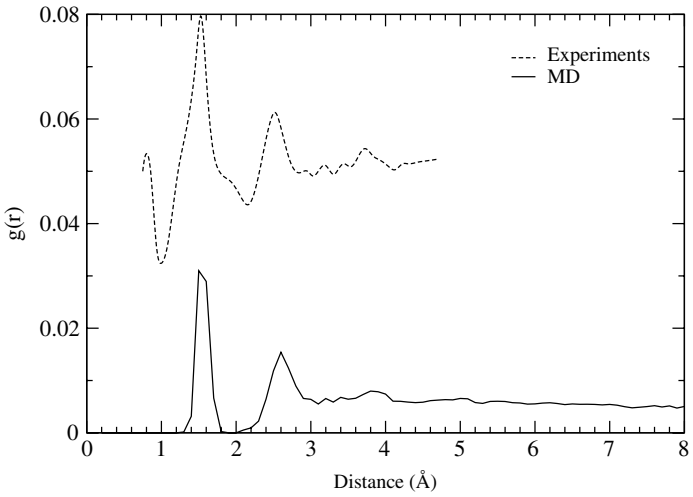

Figure 1. Radial distribution function derived from neutron scattering experiments (from [37], figure 1, curve 3) compared with the RDF of the generated MD sample.

simulation cycle. The number of hydrogen atoms (50) was determined in such a way that an increase in the number of hydrogen atoms had no detectable impact on the simulation with the present argon energy of 150 eV, since the total amount of near-surface hydrogen was in saturation; additionally incident H atoms were either reflected from the sample or simply replaced hydrogen atoms already present on the surface. Also, H abstraction and formation of H_2 molecules could be observed, but the total number of hydrogen atoms showed only small fluctuations around the saturation value.

The co-bombardment simulation was carried out in 11 equivalent sets, i.e. calculated with identical parameters but different random number initializations. Every set consisted of 13 cumulative repetitions of the (1 Ar + 50 H) co-bombardment simulation cycle plus one additional, final Ar impact. In total, the surface was bombarded by 7150 hydrogen and 154 Ar atoms in the 11 simulation sets.

For comparison, two additional sets of cumulative bombardment runs were performed with only Ar atoms and with only H atoms, respectively. These sets were organized in every respect like the co-bombardment simulation sets described before, except that bombardment by one of the projectile species was left out.

3. Results

The amorphous nature of the sample before bombardment was characterized by the RDF and compared with the data obtained from neutron scattering experiments [37], as is shown in figure 1. The location of the peaks indicating the next-neighbour (1.5 Å) and second-next-neighbour (2.8 Å) distances are in good agreement with the experimental data. Even though the less pronounced peak at 3.8 Å coincides, the influence of the finite size of the MD sample on this peak of the computed RDF has to be kept in mind. The structure below 1 Å in the measurement is due to H_2 molecule contributions present in the experimental data since the experimental RDF is given by the superposition of contributions of all atom pairs (C–C, C–H and H–H), which is also the reason for the shoulder at 2 Å. The RDF was also computed after

Table 1. Film properties before and after bombardment simulations. The quantities in brackets are for the upper half (14 Å) of the sample. The displayed values are averaged over all corresponding simulation sets and the standard deviations. Given are the numbers of C and H atoms in the sample as well as their ratio H/C. The bond distribution gives the number of C–C coordinations (for details see text).

				Bond distribution			
Sample	C	H	H/C	1C	2C	3C	4C
Initial	510	315	0.618	8	169	267	66
		(177)	(0.616)				
H only	510	346	0.678	8	169	269	64
		(208 ± 1)	(0.725)				
Ar only	499 ± 3	292 ± 4	0.584	12 ± 1	196 ± 2	260 ± 1	31 ± 1
		(154 ± 6)	(0.559)				
Ar|H	484 ± 3	323 ± 4	0.667	16 ± 1	187 ± 2	241 ± 2	39 ± 2
		(190 ± 4)	(0.715)				

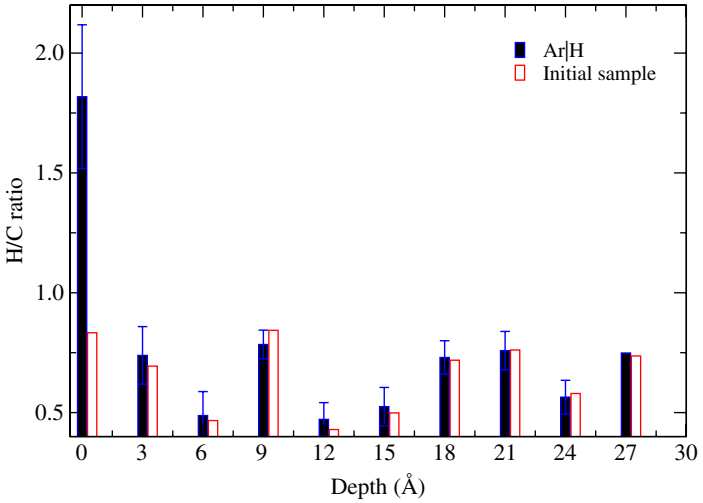

Figure 2. Average H/C ratio of the sample before and after one Ar|H simulation cycle.

bombardment and the difference with the initial RDF lies within the statistical fluctuations. This confirms that the cumulative bombardment did not significantly harm the structural integrity of the sample.

Some key properties of the sample, before and after the various bombardment events, are compared in table 1. The given numbers of atoms include only the active atoms, i.e. all atoms except those fixed at the bottom 3 Å of the sample. Since the structure of the sample is given by the network of carbon atoms from here on we refer to the carbon–carbon bond number as carbon coordination, which explicitly excludes the number of C–H bonds. It can be seen that in the case of H-only simulations the number of carbon atoms of the initial sample is unchanged by the additionally offered hydrogen, i.e. no erosion occurred. Figure 2 shows the comparison of

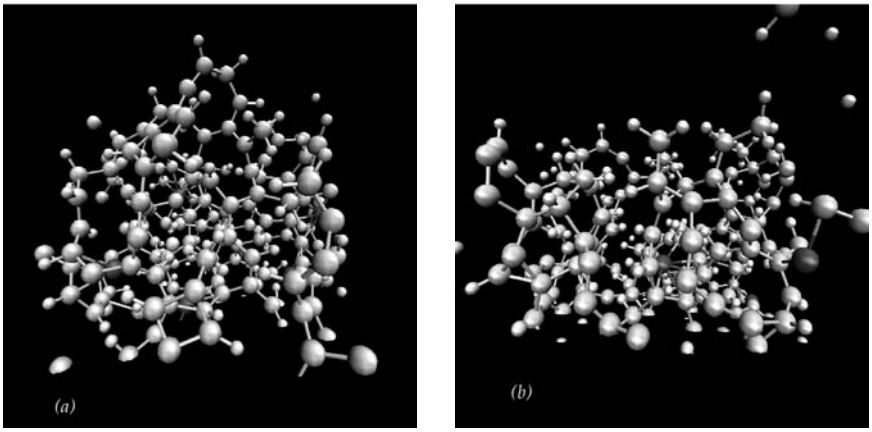

Figure 3. The surface structure after 12 Ar impacts: (a) Ar-only case, (b) Ar|H case. Representation of the sample atoms: hydrogen by small light grey spheres, argon by dark grey spheres, carbon by light grey spheres.

the H/C ratio as a function of depth for the initial sample and the Ar|H bombarded sample after one cycle of simulations (1 Ar and 50 H) averaged over 11 sets. The increase in the hydrogen content is restricted to the upper part of the sample (3 Å), forming a thin, hydrogen-enriched layer which has also been observed in other simulations [38]. Nevertheless, a comparison of the C–C bond statistics between the initial sample and the sample after H exposure reveals that the carbon network is not affected by this increase of surface H content, because most of the hydrogen atoms are added to the already existing open bonds in the initial sample. In the case of physical sputtering by Ar bombardment, an average loss of 11 C atoms has been observed, which corresponds to an erosion yield of $0.8 \pm 0.2\,\mathrm{C\,Ar^{-1}}$. The Ar bombardment increases the number of carbon atoms with a lower carbon coordination number at the expense of 4-fold coordinated carbon atoms. At the same time, the upper part is depleted of hydrogen since the average loss ratio is $\mathrm{C : H} = 1 : 2$. This depletion has also been noticed by Beardmore and Smith [39], however at Ar energies of 1 keV.

In the case of co-bombardment, on average 26 carbon atoms were lost, corresponding to a yield of $1.9 \pm 0.2\,\mathrm{C\,Ar^{-1}}$. The incident hydrogen is incorporated into the surface layer maintaining its supersaturated condition as can be seen from the H/C ratio. Taking into account the reduced number of C atoms in the sample, the bond distribution indicates the increased appearance of terminal C atoms in addition to the changes induced by the physical sputtering processes. This structural difference can be more clearly deduced from a visual comparison of the surface structures displayed in figure 3.

Figure 4 shows the distribution of added H atoms as a function of depth after 7150 impact events over 11 sets of simulations in the co-bombardment case. The energetic bombardment causes an increased surface roughness of the samples since molecule chains stick out of the surface. Furthermore, the additionally incorporated hydrogen causes some ‘swelling’ of the surface layers. This hampers the unambiguous definition of the surface location after several impact events in each individual case, but the averaged depth scale of the individual runs is sufficiently stable. After co-bombardment the sample was elongated along the z-direction to a total extension from bottom to top of up to 33.3 Å compared to its original 28 Å. The z location of the outermost atom is taken as the origin of the depth scale in all subsequent plots. Positive

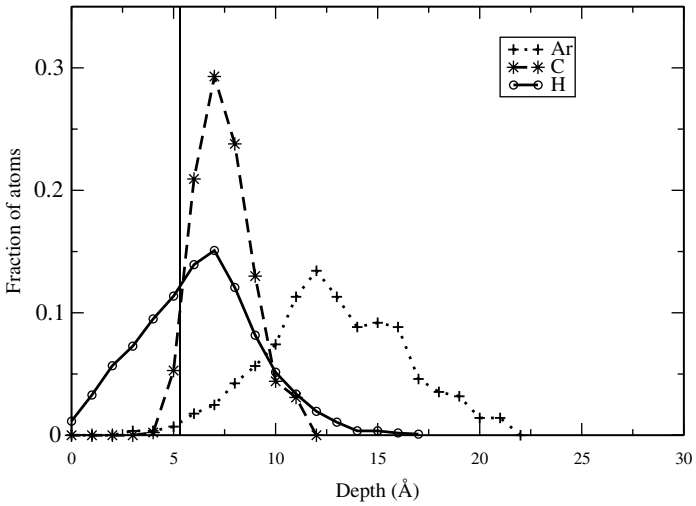

Figure 4. Distribution of implanted Ar and H projectiles and the origin of eroded C atoms within the sample in Ar|H simulations. The vertical line indicates the initial surface.

z-values lie below the surface. The mean depth of the additionally incorporated hydrogen is 6.3 Å (1 Å w.r.t. to the original surface). A huge fraction of hydrogen was reflected (6293 out of 7150), which means on average 78 new hydrogen atoms were added per simulation set. Since there was an exchange between already present hydrogen and the newly added ones, on average 52 hydrogen atoms were additionally incorporated into the sample. At the same time, 44 hydrogen atoms left the sample in eroded hydrocarbons so that only 8 additional H are found at the end of the simulation set (see table 1).

In comparison, the average number of atoms added in the H-only case is 31, which is significantly lower than in the case of Ar|H, although the mean depth of the added hydrogen is very similar (≈1.3 Å w.r.t. the original surface). This shows that the Ar bombardment did not cause additional diffusion of H atoms into the bulk at 300 K, rather it created more dangling bonds on the surface and thereby facilitated the addition of more H atoms. In both simulation sets the simulation time was 350 ps.

Furthermore, figure 4 shows the depth profile of the implanted Ar atoms along with the profile of the eroded C atoms. The mean ejection depth of the carbon atoms is about 7.5 ± 1.4 Å w.r.t. the new surface (2.3 Å w.r.t. the original surface). The distribution of the Ar atoms after being thermalized is very broad with a maximum around 12 Å. The broad distribution indicates that the individual collision cascades are very different. The depth profile of the displaced carbon atoms due to cumulative Ar bombardment is shown in figure 5. A carbon atom was considered as displaced when an initially existing C–C bond was still broken at the end of the Ar simulation set (bombardment by 14 Ar atoms). It can be seen that most of the atomic displacement happened within a distance of 6–8 Å inside the sample and the maximum of the C displacement distribution coincides with the maximum of the distribution of the eroded C atoms.

In figure 6, the variation of the numbers of atoms with carbon coordination number n (number of C–C bonds), $n = 1, \ldots, 4$, is plotted as a function of Ar impact events for the Ar|H case. The numbers are normalized to the number of carbon atoms after every Ar bombardment

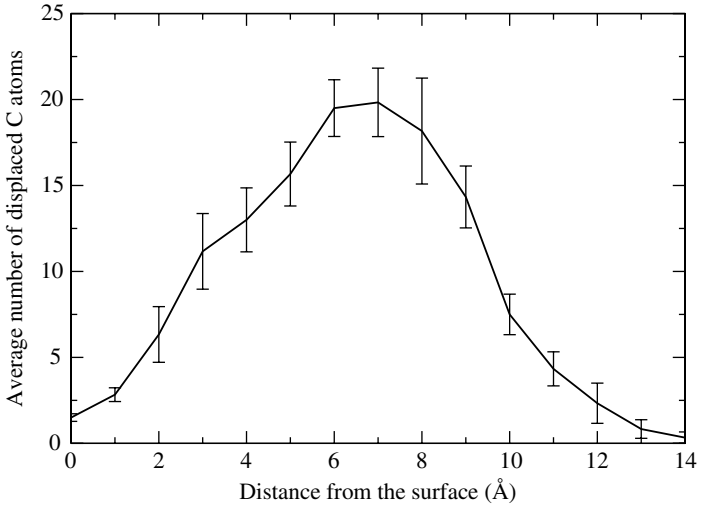

Figure 5. Depth profile of the average number of displaced carbon atoms due to Ar bombardment per simulation set (14 Ar impacts).

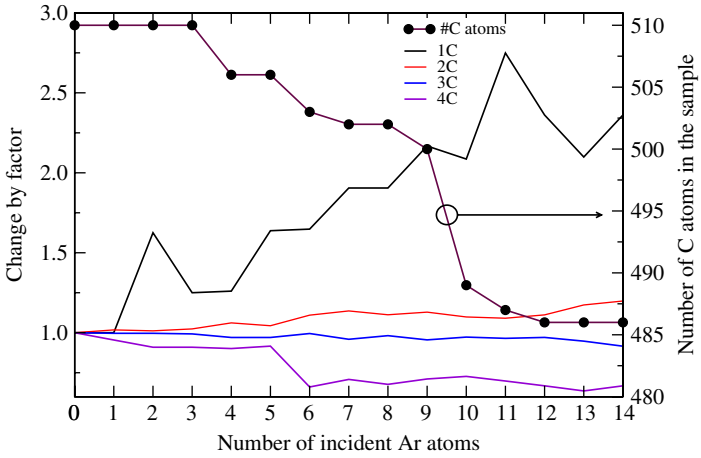

Figure 6. Carbon–carbon coordination and number of carbon atoms in the sample as a function of the number of Ar impact events in the Ar–H case. The lines without symbols show the numbers of atoms with carbon coordination number n, $n = 1, \ldots, 4$, normalized to the number of carbon atoms in the sample after each Ar impact and rescaled such that their initial values are 1.

event in the sample and rescaled such that their initial values are 1. It can be seen that the numbers of singly and doubly coordinated atoms are increased at the expense of 3- and 4-fold coordinated atoms. The analysis of the sputtered species for the Ar-alone and Ar|H cases are shown in figure 7. The erosion histogram shows the fraction of different ejected hydrocarbon radicals normalized to the total number of ejection events. It can be seen that the fraction of C_xH_y, where $x > 3$, is small in both cases. Nevertheless, the fraction of eroded C_2 and C_3 molecules is significantly higher if additional hydrogen is present. No carbon erosion was observed in pure hydrogen bombardment simulations.

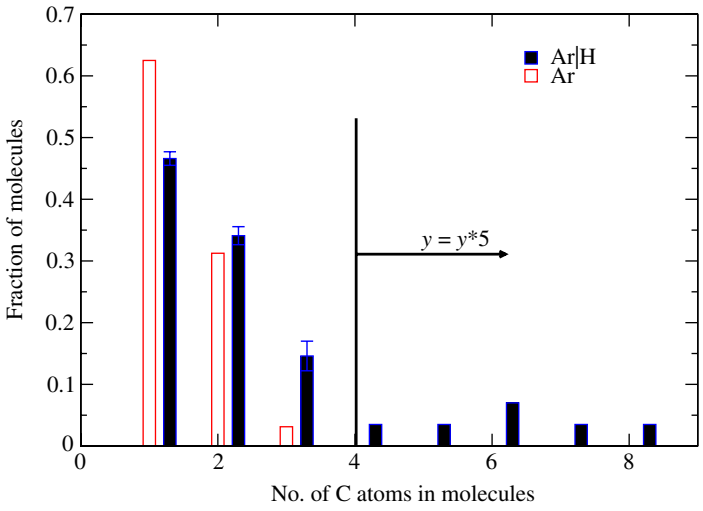

Figure 7. Distribution of the number of carbon atoms in the sputtered molecules in both Ar|H and Ar-only cases.

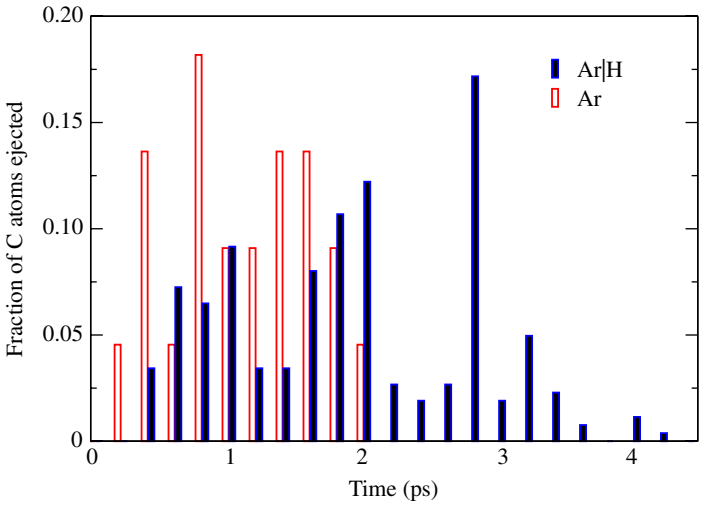

Figure 8. Histogram of the emission time of eroded carbon atoms after the Ar impact. Most of the larger molecules were eroded at later times (>2.5 ps), contributing a high fraction to the number of carbon atoms.

Figure 8 is the temporal profile of carbon atoms ejected in the form of C_xH_y molecules. It can be seen that all of the carbon atoms were ejected within a time of 5 ps after bombardment. A closer inspection of the emission time reveals that most of the smaller hydrocarbons (C_1H_y) were ejected within 1 ps after the Ar impact. Most of the larger molecules were eroded at later times (> 2.5 ps), contributing a high fraction of the eroded carbon atoms in the case of Ar|H simulations. In the Ar-only case, the lack of molecules with more than three C atoms (see figure 7) prevents the occurrence of any late emissions.

Figure 9 shows the kinetic energy distribution of the ejected C_xH_y molecules, for $x \in \{1, 2, 3, 4\}$. The kinetic energy of the eroded molecules is above thermal energy in nearly all

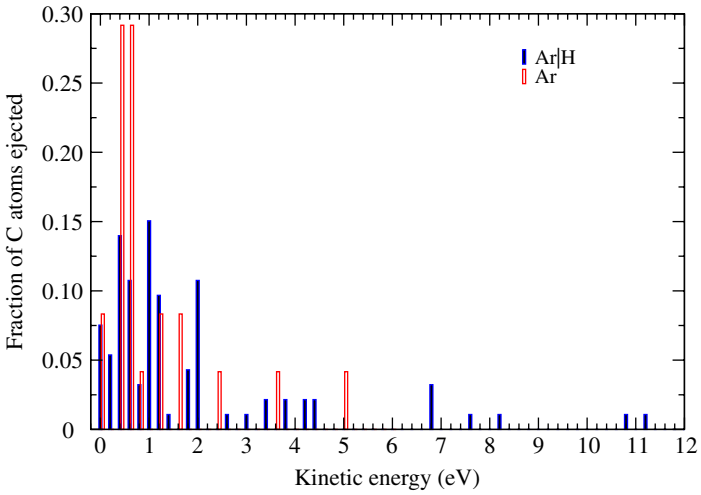

Figure 9. Energy distribution of sputtered carbon atoms. The high energy tail in the Ar|H case indicates the increased fraction of loosely bound C atoms.

cases and the emission is therefore a direct consequence of the ion impact in both the Ar only and the co-bombardment cases. The energy of the higher hydrocarbons ($x \geqslant 3$) is also above the thermal range (0.5–2 eV). The high energy tail in the Ar|H simulations is due to the more pronounced occurrence of loosely bound carbon atoms.

4. Discussion

In the case of bombardment by Ar only, we observed physical sputtering with a yield of 0.8 ± 0.2 C/Ar. For comparison, TRIM.SP [21] calculations were performed for a sample with the density and stoichiometry of the initial MD sample; they predict a yield of 0.47. In these calculations, the surface binding energy for carbon was set to 2.8 eV because it is known that this value leads to good agreement with experimental data for the physical sputtering of a-C:H films with 30% hydrogen at perpendicular incidence [16]. When comparing the TRIM.SP value to the MD yield it should be kept in mind, that the experimental yields were measured in steady state with a surface partly depleted of hydrogen due to the ion bombardment. Therefore, for the initial sputtering of a hydrogen-rich fresh film like the MD sample a somewhat increased sputtering yield is to be expected.

In the co-bombardment case, we observed the ejection of unsaturated radicals from a-C:H layers at 300 K surface temperature with a much higher yield of 1.9 ± 0.2. This can be attributed to the abundance of hydrogen in the top layers of the film. The process of erosion can be described as follows: Ar atoms create open bonds within their penetration range (mean range ≈ 8 Å) resulting in the formation of linear hydrocarbon chains. The fractions of singly and doubly coordinated atoms are increased at the expense of 3- and 4-fold coordinated atoms, as shown in figure 6. The damage created is mostly in the top layers, as can be seen from the depth profile of the displaced atoms (figure 6), which is in reasonable agreement with TRIM.SP calculations [13]. In the case of the Ar|H simulations, the open bonds in the top layers are passivated due to hydrogen bombardment, resulting in hydrogen-rich upper layers. This can be seen from the H/C ratio of the top layers of the film which is given in table 1 and figure 2

for both the Ar-alone and Ar|H cases. The surface structure of the film after 12 Ar impacts for both the Ar-alone and Ar|H cases is shown in figure 3. In the case of pure Ar bombardment, the long hydrocarbon chains get closed via re-attachment at some other open bond locations. However, the screening effect of hydrogen atoms in the Ar|H case makes the closing of long hydrocarbon chains difficult even if there are available binding sites. Although this effect is hard to quantify it is clearly visible in the simulations. Nevertheless, the resulting effect can be seen in the bond variation as shown in table 1. The steric repulsion arising between H atoms connected to different C atoms keeps the linear chains straight in the case of Ar|H simulations.

The subsequent Ar impacts cause further breaking of C–C bonds resulting in the detachment of unsaturated molecules from the sample. The bond breaking was either by direct bombardment or by the knock-on atoms. Since the outermost atoms of the linear carbon chains are covered with hydrogen in the Ar|H case, the detached molecule fails to re-attach to any other available bonding site. Hence, the unsaturated molecule leaves the sample. As can be seen from the temporal distribution of the eroded particles, all of the molecules were ejected within 5 ps after Ar impact. The kinetic energy distribution of the eroded particles (see figure 9) shows that the ejected molecules are not thermalized. None of the emitted carbon atoms came out as CH_4 in either the Ar-alone or Ar|H simulations. The analysis of the sputtered species in each case shows that the fraction of radicals having more than 4 carbon atoms is low, which is in agreement with the existing results for co-bombardment simulations performed with low energy noble gas ions and hydrogen atoms (5 and 10 eV) on a-C:H films [40].

The chemical and momentum transfer effects involved in the erosion process can be clearly distinguished. The ejection of C_xH_y radicals is entirely a momentum transfer effect. The erosion of unsaturated hydrocarbon radicals from deuterated amorphous carbon layers at 300 K due to 100 eV deuterium ion bombardment has been reported recently by Marian *et al* [25]. The mechanism of erosion is physical sputtering, as in the final emission step of the present case. However, the steric repulsion which arises due to excess hydrogen on the surface in our simulations is purely chemical in origin and is responsible for the increased sputtering yield.

The profile of the initial locations of the eroded carbon atoms within the sample shows that the erosion happens from the top layers (mean depth $\approx$ 6 Å w.r.t. the modified surface). Most of the sample remains undisturbed since the displaced C atoms are localized within a few angstrom of the surface as shown in figure 5. The profile of added hydrogen atoms (figure 4) shows that they are mainly confined to a few surface layers. Diffusion effects are not prominent on the simulation timescales. The observed erosion timescales ($\approx$ ps) are much faster than the typical molecular diffusion time ($\approx \mu$s). Unlike a-C:H layers, diffusion could be a dominant mechanism for the structurally different hydrogenated graphite, as reported by Vietzke [41]. The detailed study of diffusion processes requires algorithms capable of handling longer timescales than MD, which is not in the scope of the present study.

5. Conclusion

The molecular dynamics simulations show an increased carbon erosion yield of a-C:H layers due to the bombardment of energetic argon atoms in the presence of very-low-energy hydrogen atoms, as compared to physical sputtering by argon ions only. This increase of the erosion yield has also been observed in experiments [13].

The mechanism which leads to the yield enhancement in the simulations, *hydrogen enhanced physical sputtering* (*HEPS*), can be described by the following steps: first, the

energetic argon ions create dangling bonds within the penetration range. Then the abundant hydrogen atoms saturate most of the broken bonds in the first few atomic layers. Subsequent Ar bombardment causes the breaking of more C–C bonds. Up to this point the observed mechanism coincides with the atomistic model proposed in [13, 14], where it is also assumed that the ion bombardment breaks C–C bonds and hydrogen attachment prevents the recombination of the broken bonds. However, in the MD simulations, we see that the steric repulsion which arises from H atoms bound to neighbouring C atoms in the top layer plays an important role in preventing the recombination of broken C–C bonds. Finally, the release of hydrocarbon molecules is caused by a physical sputtering step. Hence, the emitted molecules are energetic radicals as opposed to the thermalized and saturated hydrocarbon molecules proposed by Hopf *et al* [14].

The HEPS mechanism is a fast surface erosion process and the timescales are in the picosecond range. Within the total time of 4.3 ns of the cumulative simulations no indication of diffusion of isolated saturated hydrocarbon molecules could be detected and the relative ratio of the experimental and simulated yields for physical sputtering and HEPS do not indicate the need for additional mechanisms to explain the experimental data. On the other hand, we cannot exclude the possibility that the diffusion process suggested in [14] may contribute on timescales (ms) not accessible with MD simulations.

In future studies, the dependence of the erosion yield on the Ar/H ratio, the argon energy and the angle of incidence will be examined.

Acknowledgments

We thank Drs S P Deshpande, W Jacob, Th Schwarz-Selinger and M Warrier for inspiring and useful discussions. We also thank Professor K Nordlund for providing the HCPARCAS code, helpful comments on the manuscript and hospitality during an extended visit at the accelerator laboratory of the University of Helsinki. The research was supported and partly funded by the DST/DAAD collaboration on ‘Hydrogen co-deposition: numerical simulations and experiments’.

References

[1] Federici G *et al* 2001 Plasma–material interactions in current tokamaks and their implications for next step fusion reactors *Nucl. Fusion* **41** 1967–2137

[2] Mayer M, Rohde V and von Keudell A and ASDEX Upgrade Team 2003 Characterisation of deposited hydrocarbon layers below the divertor and in the pumping ducts of ASDEX Upgrade *J. Nucl. Mater.* **313–316** 429–33

[3] Roth J 1999 Chemical erosion of carbon based materials in fusion devices *J. Nucl. Mater.* **266–269** 51–7

[4] Jacob W and Roth J 2007 Chemical sputtering *Sputtering by Particle Bombardment IV (Topics in Applied Physics* vol 10) ed R Behrisch and W Eckstein (Berlin: Springer) pp 329–400

[5] Denisov V N, Kuzik L A, Lvova N, Mavrin B N, Opimach I V, Popov M and West W P 1998 Hard diamond-like layers produced during DIII-D tokamak operations *Phys. Lett.* A **239** 328–31

[6] Jacob W 2005 Redeposition of hydrocarbon layers in fusion devices *J. Nucl. Mater.* **337–339** 839–46

[7] Mayer M, Balden M and Behrisch R 1998 Deuterium retention in carbides and doped graphites *J. Nucl. Mater.* **252** 55–62

[8] Roubin P, Martin C, Arnas C, Colomban Ph, Pégourié B and Brosset C 2005 Raman spectroscopy and x-ray diffraction studies of some deposited carbon layers in Tore Supra *J. Nucl. Mater.* **337–339** 990–4

[9] Sharma A R, Schneider R, Toussaint U and Nordlund K 2007 Hydrocarbon radicals interaction with amorphous carbon surfaces *J. Nucl. Mater.* **363–365** 1283–8
[10] Roth J and Bohdansky J 1987 Sputtering of graphite with light ions at energies between 20 and 1000 eV *Nucl. Instrum. Methods* B **23** 549–51
[11] Balden M and Roth J 2000 New weight-loss measurements of the chemical erosion yields of carbon materials under hydrogen ion bombardment *J. Nucl. Mater.* **280** 39–44
[12] Vietzke E, Flaskamp K and Philipps V 1982 Hydrocarbon formation in the reaction of atomic hydrogen with pyrolytic graphite and the synergistic effect of argon ion bombardment *J. Nucl. Mater.* **111–112** 763–8
[13] Hopf C, von Keudell A and Jacob W 2003 Chemical sputtering of hydrocarbon films *J. Appl. Phys.* **94** 2373–80
[14] Hopf C, von Keudell A and Jacob W 2002 Chemical sputtering of hydrocarbon films by low-energy Ar^+ ion and H atom impact *Nucl. Fusion* **42** L27–L30
[15] Hopf C and Jacob W 2005 Bombardment of graphite with hydrogen isotopes: a model for the energy dependence of the chemical sputtering yield *J. Nucl. Mater.* **342** 141–7
[16] Jacob W, Hopf C and Schlüter M 2006 Chemical sputtering of carbon materials due to combined bombardment by ions and atomic hydrogen *Phys. Scr.* **T124** 32–6
[17] Küppers J 1995 The hydrogen surface chemistry of carbon as a plasma facing material *Surf. Sci. Rep.* **22** 249–321
[18] Eckstein W and Philipps V 1996 Physical sputtering and radiation-enhanced sublimation *Physical Processes of the Interaction of Fusion Plasmas with Solids (NATO-ASI Series B: Physics)* (New York: Academic) pp 93–133
[19] Eckstein W 1998 Sputtering, reflection and range values for plasma edge codes. Technical Report IPP 9/117, Max-Planck-Institut für Plasmaphysik, Garching
[20] Eckstein W and Preuss R 2003 New fit formulae for the sputtering yield *J. Nucl. Mater.* **320** 209–213
[21] Eckstein W 1991 *Computer Simulation of Ion–Solid Interactions* (*Springer Series in Materials Science* vol 10) 1st edn (Berlin: Springer)
[22] Salonen E, Nordlund K, Keinonen J and Wu C H 2001 Swift chemical sputtering of amorphous hydrogenated carbon *Phys. Rev.* B **63** 195415
[23] Nordlund K 2004 Atomistic simulation of radiation effects in carbon-based materials and nitrides *Nucl. Instrum. Methods* B **218** 9–18
[24] Nordlund K, Salonen E, Krasheninnikov A V and Keinonen J 2006 Swift chemical sputtering of covalently bonded materials *Pure Appl. Chem.* **78** 1203–11
[25] Marian J, Zepeda-Ruiz L A, Couto N, Bringa E M, Gilmer G H, Stangeby P C and Rognlien T D 2007 Characterization of sputtering products during graphite exposure to deuterium ions by molecular dynamics *J. Appl. Phys.* **101** 044506
[26] Meyer F W, Krstic P S, Vergara L I, Krause H F, Reinhold C O and Stuart S J 2007 Low energy chemical sputtering of ATJ graphite by atomic and molecular deuterium ions *Phys. Scr.* **T128** 50–4
[27] Krstic P S, Reinhold C O and Stuart S J 2007 Chemical sputtering from amorphous carbon under bombardment by deuterium atoms and molecules *New J. Phys.* **9** 209
[28] Stuart S J, Krstic P S, Embry T A and Reinhold C O 2007 Methane production by deuterium impact at carbon surfaces *Nucl. Instrum. Methods* B **255** 202–7
[29] Nordlund K, Keinonen J and Mattila T 1996 Formation of ion irradiation induced small-scale defects on graphite surfaces *Phys. Rev. Lett.* **77** 699–702
[30] Brenner D W 1990 Empirical potential for hydrocarbons for use in simulating the chemical vapour deposition of diamond films *Phys. Rev.* B **42** 9458–71
[31] Brenner D W 1996 Chemical dynamics and bond-order potentials *MRS Bull.* **21** 36–41
[32] Träskelin P, Nordlund K and Keinonen J 2006 H, He, Ne, Ar-bombardment of amorphous hydrocarbon structures *J. Nucl. Mater.* **357** 1–8

[33] Berendsen H J C, Postma J P M, Van Gunsteren W F, DiNola A and Haak J R 1984 Molecular dynamics with coupling to an external bath *J. Chem. Phys.* **81** 3684–90
[34] Schwarz-Selinger T, von Keudell A and Jacob W 1999 Plasma chemical vapor deposition of hydrocarbon films: the influence of hydrocarbon source gas on the film properties *J. Appl. Phys.* **86** 3988–96
[35] Robertson J 2002 Diamond-like amorphous carbon *Mater. Sci. Eng.* R **37** 129–281
[36] Ziegler J F, Biersack J P and Littmark U 1985 *The Stopping and Range of Ions in Solids* vol 1 (New York: Pergamon)
[37] Walters J K and Newport R J 1995 The atomic-scale structure of amorphous hydrogenated carbon *J. Phys.: Condens. Matter* **7** 1755–69
[38] Salonen E, Nordlund K, Tarus J, Ahlgren T, Keinonen J and Wu C H 1999 Suppression of carbon erosion by hydrogen shielding during high-flux hydrogen bombardment *Phys. Rev.* B **60** 14005–8
[39] Beardmore K and Smith R 1995 Ion bombardement of polyethylene *Nucl. Instrum. Methods* B **102** 223–7
[40] Träskelin P, Nordlund K and Keinonen J 2005 He, Ne, Ar-bombardment of carbon first wall structures *Nucl. Instrum. Methods* B **228** 319–24
[41] Vietzke E 2001 Energy distributions of CD_4 and CD_3 chemically released from graphite by D^+ and D^0/Ne^+ impact *J. Nucl. Mater.* **290–293** 158–61